Open quantum system description of singlet-triplet qubits in quantum dots

L. K. Castelano,[1,*] F. F. Fanchini,[2,3] and K. Berrada[3,4]

[1]*Departamento de Física, Universidade Federal de São Carlos, 13565-905 São Carlos, SP, Brazil*

[2]*Faculdade de Ciências, UNESP–Universidade Estadual Paulista, Bauru, SP 17033-360, Brazil*

[3]*The Abdus Salam International Centre for Theoretical Physics, Strada Costiera 11, Miramare-Trieste, Italy*

[4]*Physics Department, College of Science, Al Imam Mohammad Ibn Saud Islamic University (IMISU), Riyadh, Saudi Arabia*

(Received 27 March 2015; revised manuscript received 19 August 2016; published 23 December 2016)

We develop a theoretical model to describe the dissipative dynamics of singlet-triplet qubits in GaAs quantum dots. Using the concurrence experimentally obtained [Shulman *et al.*, Science **336**, 202 (2012)] as a guide, we assume that each logical qubit fluctuates under the action of a random telegraph noise (RTN) that simulates the $1/f^{\alpha}$ noise. We also study the dynamics of concurrence as a function of the amplitude of the RTN, the correlation time of the RTN, the preparation time of states, and the two-qubit coupling. Furthermore, we show that the two-qubit coupling together with the preparation time strongly affect the entanglement dissipative dynamics and both physical quantities can be employed to enhance the entanglement between singlet-triplet qubits.

DOI: 10.1103/PhysRevB.94.235433

I. INTRODUCTION

The development of quantum information processing has enabled the discovery of new techniques and platforms which are paving the way to accomplish quantum technologies in the near future [1]. Among these platforms, spin qubits in quantum dots (QDs) [2] is certainly one of the most striking systems because of their potential scalability and miniaturization [3–5]. Furthermore, electrical readout and control of spin qubits in QDs have been achieved in several different approaches [6], where spin blockade and charge sensors enable the observation of single/two-spin dynamics [7]. In double quantum dots (DQDs), a logical qubit can be encoded by means of singlet-triplet (S-T_0) states of two electron spins [8–10] and the interqubit interaction can be implemented through a capacitive coupling [11]. By controlling and coupling S-T_0 qubits, the entanglement between two S-T_0 qubits has been experimentally demonstrated [12]. Together with the success of such a demonstration, the ubiquitous noise has been probed in the experimental data of Ref. [12]. For a single S-T_0 qubit, the noise has been characterized and shown to be consistent with the power-law $1/f^{\alpha}$ noise [13]. Also, it has been experimentally verified that the exponent α has a temperature dependence; for instance, $\alpha \approx 0.7$ for $T = 50$ mK and $\alpha \approx 0$ for $T = 100$ mK [13]. Such a temperature dependence can be ascribed to a phonon-induced decoherence mechanism [14]. The $1/f^{\alpha}$ noise can be present in a variety of systems [15] and particularly in other QD systems [16,17]. To model the $1/f^{\alpha}$ noise, random telegraph noise (RTN) has been employed in different theoretical works [18–21].

In this work, we employ the RTN to describe the decoherence caused by the interaction between two S-T_0 qubits and their environment in the low temperature limit, i.e., $\alpha \neq 0$. By using such a model, we are able to quantitatively reproduce experimental results obtained for S-T_0 qubits in two GaAs coupled DQDs [12]. Through our description of this open quantum system, we exploit the role of the amplitude of the RTN, the correlation time of the RTN, the preparation time of states, and the two-qubit coupling in the entanglement dissipative dynamics.

The present paper is organized as follows. In the next section, we present the model that describes the dynamics of the open quantum system. In Sec. III, we introduce the concept of entanglement, measured by concurrence, together with the results of our theoretical model. We also include in Sec. III a detailed study on the most important physical parameters that rule the entanglement dynamics. Finally, Sec. IV contains a summary of our results.

II. THEORETICAL MODEL

The main focus of this work is related to the study of the dissipative dynamics of two S-T_0 qubits, where the information is stored in the spin states of two electrons. Such states can be experimentally achieved by confining two electrons in each DQD system [12]. The logical qubit composed by the two-level system ($|S\rangle \equiv |\uparrow\rangle, |T_0\rangle \equiv |\downarrow\rangle$) can be isolated by applying an external magnetic field in the plane of the device in such a way that the Zeeman splitting makes the parallel spin states $|T_+\rangle$ and $|T_-\rangle$ energetically inaccessible.

To extend such a two-level system to a two-qubit system, it is necessary to couple two S-T_0 qubits, where the tunneling between them is suppressed and their coupling is electrostatic (for more details, see Ref. [12]). Thus, the effective Hamiltonian for the two-qubit system can be written as follows [12]:

$$\begin{aligned}\hat{H}_{2\text{-qubit}} = {} & \frac{1}{2}\left(J_1\sigma_z^{(1)}\otimes\mathbf{I} + J_2\,\mathbf{I}\otimes\sigma_z^{(2)}\right) \\ & + \frac{J_{12}}{4}\left(\sigma_z^{(1)}\otimes\sigma_z^{(2)} - \sigma_z^{(1)}\otimes\mathbf{I} - \mathbf{I}\otimes\sigma_z^{(2)}\right) \\ & + \frac{1}{2}\left(\Delta B_{z,1}\sigma_x^{(1)}\otimes\mathbf{I} + \Delta B_{z,2}\,\mathbf{I}\otimes\sigma_x^{(2)}\right), \qquad (1)\end{aligned}$$

where $\sigma_{x,y,z}$ are the Pauli spin matrices, $\mathbf{I}$ is the identity, and the index 1 (2) is related to the first (second) qubit (hereafter, we use units of $\hbar = 1$). This Hamiltonian is able to implement universal quantum control, which is given by two physically distinct local operations, x and z, and by the interaction between the qubits given by $\sigma_z^{(1)}\otimes\sigma_z^{(2)}$. The exchange splitting, J_i, between $|S^i\rangle$ and $|T_0^i\rangle$ applies rotations in the qubit

*lkcastelano@ufscar.br

$i = 1,2$ around the z axis, while rotations around the x axis are driven by a magnetic field gradient ΔB_z. Moreover, ΔB_z is responsible for the preparation of each qubit in a superposition between $|S\rangle$ and $|T_0\rangle$. The two-qubit coupling, J_{12}, depends on the energy between levels of the left and the right DQD and it can be switched on and off during the quantum dynamics [12]. Due to the Pauli exclusion principle, $|S\rangle$ and $|T_0\rangle$ states have different charge configurations and because both qubits are electrostatically coupled, the state of the first qubit is conditioned to the state of the second qubit. In other words, when simultaneously evolving, they experience a dipole-dipole coupling that generates an entangled state. Following the experimental steps [12], each qubit is initialized in the $|S\rangle$ state, then rotated by $\pi/2$ around the x axis when $J_i = J_{12} = 0$, $\Delta B_{z,i}/2\pi \approx 30$ MHz, for $i = 1,2$. After this stage, a large exchange splitting is switched on corresponding to $J_1/2\pi \approx 280$ MHz, and $J_2/2\pi \approx 320$ MHz. Experimentally, it was found that the two-qubit coupling is given by $J_{12} = J_1 J_2$ [12].

To include the dissipative dynamics, we consider a phenomenological approach, where both qubits are subjected to local RTN fluctuations on exchange splitting terms J_1 and J_2. Thus, the RTN Hamiltonian can be written as

$$\hat{H}_{\rm RTN} = J_1^{\rm RTN}(t,\tau_c)\sigma_z^{(1)} \otimes \mathbf{I} + J_2^{\rm RTN}(t,\tau_c)\mathbf{I} \otimes \sigma_z^{(2)}. \quad (2)$$

For such kind of noise, $J_k^{\rm RTN}(t,\tau_c)$ jumps between two values $-J_0$ and J_0 according to [18]

$$J_k^{\rm RTN}(t,\tau_c) = (-1)^{f(t,\tau_c,k)} J_0, \quad (3)$$

where $k = 1,2$ and the function $f(t,\tau_c,k)$ is related to the times where the jumps occur by the following expression:

$$f(t,\tau_c,k) = \sum_j \Theta\left(t - t_j^k\right), \quad (4)$$

where $\Theta(x)$ is the Heaviside function and

$$t_j^k = -\sum_{n=1}^{j} \tau_c \log\left(p_n^k\right). \quad (5)$$

In Eq. (5), p_n^k are uniformly distributed random numbers and the correlation time τ_c determines the frequency of jumps and is related to the autocorrelation function as follows:

$$\left\langle J_k^{\rm RTN}(t,\tau_c) J_k^{\rm RTN}(t',\tau_c)\right\rangle = \exp(-2|t-t'|/\tau_c), \quad (6)$$

where $\langle\cdots\rangle$ represents an average over the fluctuations.

III. RESULTS

The results for the $J_1^{\rm RTN}(t,\tau_c)$ are shown in Fig. 1, considering $J_0 = 1$ MHz and $\tau_c = 10$ ns (black solid curve in the top panel) and $\tau_c = 30$ ns (red dashed curve in the bottom panel). As expected, there are less jumps for a higher value of τ_c. Furthermore, to check the $1/f^\alpha$ nature of the RTN, we numerically calculate the power spectrum $S(f)$, which is the Fourier transform of the autocorrelation function [Eq. (6)]. Such results are shown in Fig. 2 for a fixed amplitude $J_0 = 1$ MHz and for different correlation times: $\tau_c = 1$ ns (magenta dotted curve), $\tau_c = 10$ ns (black solid curve), and $\tau_c = 30$ ns (blue dashed curve). The solid red curve in Fig. 2 is a plot of the function $4 \times 10^{-3}/f^{0.89}$, which is used for comparison to the high frequency behavior of the numerically

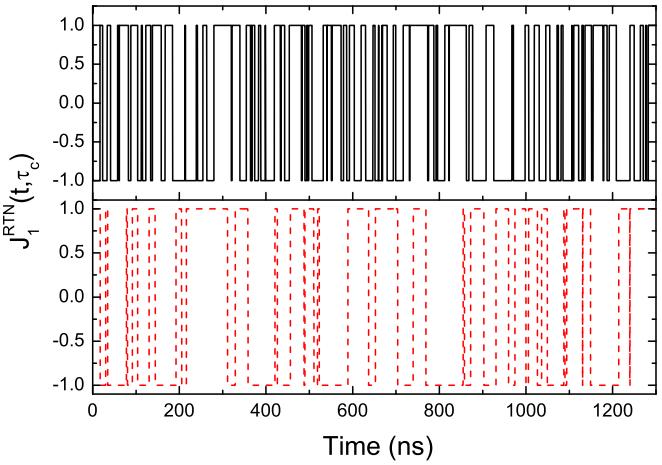

FIG. 1. Simulation of the RTN as a function of time, considering the amplitude $J_0 = 1$ MHz and two different correlation times: $\tau_c = 10$ ns (top panel) and $\tau_c = 30$ ns (bottom panel).

calculated power spectrum $S(f)$. Such a power-law noise model is similar to the one deduced for only one qubit in DQDs [13].

To perform the analysis of our results and to compare to the experimental work [12], the quantum correlation called concurrence is employed. Concurrence is a well known measure of entanglement, which is broadly accepted to be responsible for a set of important tasks in quantum information theory, such as quantum teleportation [22] and quantum key distribution [23]. For two qubits, there is an analytical solution to concurrence [24], which is given by

$$C(\rho) = \max\{0,\lambda_1 - \lambda_2 - \lambda_3 - \lambda_4\}, \quad (7)$$

where λ_i $(i = 1,2,3,4)$ are the eigenvalues of $R = \sqrt{\sqrt{\rho}\tilde{\rho}\sqrt{\rho}}$ listed in descending order. $\tilde{\rho}$ is the time-reversed density

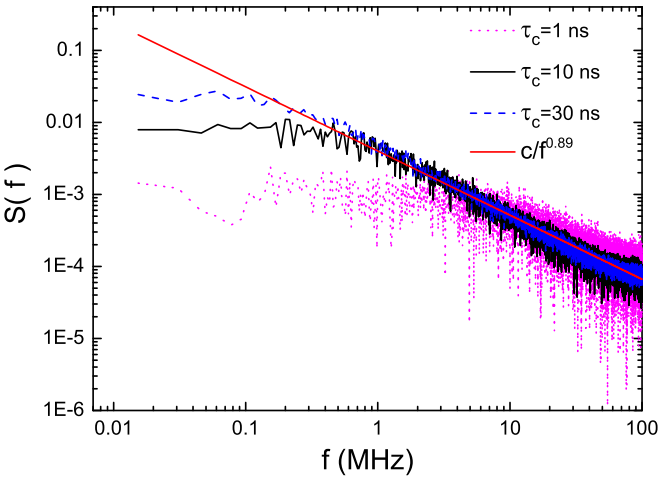

FIG. 2. Numerical calculation of the power spectrum $S(f)$ considering the RTN amplitude $J_0 = 1$ MHz and the following values for the correlation time: $\tau_c = 1$ ns (magenta dotted curve), $\tau_c = 10$ ns (black solid curve), and $\tau_c = 30$ ns (blue dashed curve). The function $c/f^{0.89}$ is plotted as a solid red curve for comparison with the high frequency limit of the numerical calculated power spectrum $S(f)$.

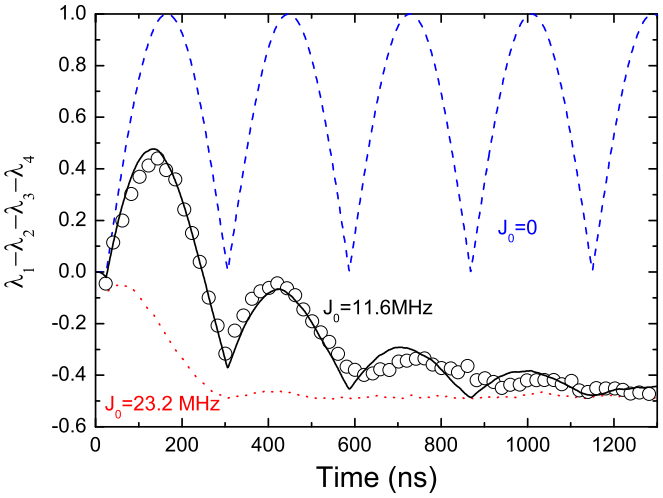

FIG. 3. Time-evolution of the DDSE considering the RTN with fixed correlation time $\tau_c = 9$ ns and for different noise amplitudes: $J_0 = 0$ (dashed blue curve), $J_0 = 11.6$ MHz (solid black curve), and $J_0 = 23.2$ MHz (dotted red curve). Open circles denote the DDSEs extracted from experimental data [12].

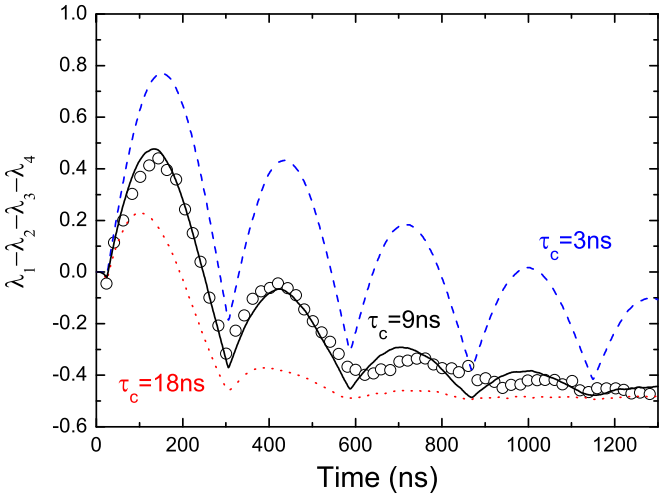

FIG. 4. Time-evolution of the DDSE considering the RTN with fixed noise amplitude $J_0 = 11.6$ MHz and for different values of the correlation time: $\tau_c = 3$ ns (dashed blue curve), $\tau_c = 9$ ns (solid black curve), and $\tau_c = 18$ ns (dotted red curve). Open circles denote the DDSEs extracted from experimental data [12].

operator, which can be written as

$$\tilde{\rho} = \left(\sigma_y^{(1)} \otimes \sigma_y^{(2)}\right)\rho^*\left(\sigma_y^{(1)} \otimes \sigma_y^{(2)}\right), \tag{8}$$

where ρ^* is the conjugate of ρ in the standard basis of two qubits.

The initial state of each DQD is set to $|\uparrow\rangle = |S\rangle$, then a $\pi/2$ rotation around the x axis is performed during the preparation time τ_{prep}, which puts each qubit in a superposed state $(|\uparrow\rangle + |\downarrow\rangle)/\sqrt{2}$. Following the experimental description given in Ref. [12], we use $\Delta B_{z,1} = \Delta B_{z,2} = \pi/(2\tau_{\text{prep}})$, $J_1/2\pi = 280$ MHz, and $J_2/2\pi = 320$ MHz. The system dynamics can be obtained by numerically solving the unitary trajectories described by the system Hamiltonian [Eq. (1)] together with the RTN Hamiltonian [Eq. (2)]. We perform an average over different unitary trajectories to extract the dynamics of the system including the RTN [25].

We begin our analysis of the dynamics of the system through the evolution in time of the difference of the descending sorted eigenvalues (DDSEs) $\lambda_1 - \lambda_2 - \lambda_3 - \lambda_4$ of the matrix $R = \sqrt{\sqrt{\rho}\tilde{\rho}\sqrt{\rho}}$, which is equal to the concurrence $C(\rho)$ when it assumes positive values. In Fig. 3, we plot $\lambda_1 - \lambda_2 - \lambda_3 - \lambda_4$ as a function of time, assuming different values for the RTN amplitude J_0 and for $\tau_c = 9$ ns. When $J_0 = 0$, the dynamics is unitary and the concurrence oscillates without dissipation with a period of 280 ns after τ_{prep}. Such a period is completely defined by the system Hamiltonian term $J_{12}/4\sigma_z^{(1)} \otimes \sigma_z^{(2)}$. DDSEs assume zero values for $t \leqslant \tau_{\text{prep}}$ when $J_0 = 0$, but the first experimental value of DDSEs at $t = 25$ ns is negative and it must be related to noise effects that occur during the preparation of the state $(|\uparrow\rangle + |\downarrow\rangle)/\sqrt{2}$. Such a negative value occurs during the preparation time as a result of the interaction of the $\pi/2$ rotation around the x direction and the RTN, which acts in the z direction. Indeed, to take into account such a negative value of DDSEs, we just need to use $\tau_{\text{prep}} = 25$ ns and $J_0 \neq 0$, as can be observed in Fig. 3.

Furthermore, one can see in Fig. 3 that the DDSE oscillates in time and it has an envelope function that decays faster as the value of J_0 is increased. We also perform an analysis of DDSEs as a function of time for a fixed value of the RTN amplitude $J_0 = 11.6$ MHz and different correlation times τ_c, which is shown in Fig. 4. The increasing of the correlation time has a similar effect when compared to the increasing of the RTN amplitude in Fig. 3; i.e., the bigger the correlation time, the faster the decay of the envelope function as a function of time. For $\tau_c = 9$ ns and $J_0 = 11.6$ MHz, there is good agreement between the experimental results (open circles in Figs. 3 and 4) and DDSEs extracted from the dynamics including the RTN. The results shown in Figs. 3 and 4 might suggest that it is possible to find different pairs of τ_c and J_0 that adjust the experimental data, but this conception is misleading because other pairs of τ_c and J_0 cannot reproduce the experimental data in the whole range of time.

By means of our description of the decoherence mechanism, we can analyze the entanglement dissipative dynamics through our theoretical model. Particularly, we focus on two aspects: the role of the preparation time τ_{prep} and the two-qubit coupling J_{12}. The system is interacting with the environment during the preparation time, which affects the entanglement efficiency. To understand the role of such a physical parameter, we analyze the effects on the maximum value of concurrence caused by distinct preparation times τ_{prep}. Another crucial physical parameter that rules the entanglement is the coupling between each qubit. The two-qubit coupling J_{12}, which can be increased by controlling the dipole-dipole interaction, determines the time τ_{ent} for achieving the state with the highest value of entanglement (concurrence). This time τ_{ent} can be extracted from the term $J_{12}/4\sigma_z^{(1)} \otimes \sigma_z^{(2)}$ of Eq. (1) and is given by $J_{12} = \pi/\tau_{\text{ent}}$. In the experimental results, $\tau_{\text{ent}}^{\text{exp}} = 140$ ns and the maximum obtained value for entanglement is around 0.44 [12]. In other words, both τ_{prep} and τ_{ent} are two fundamental

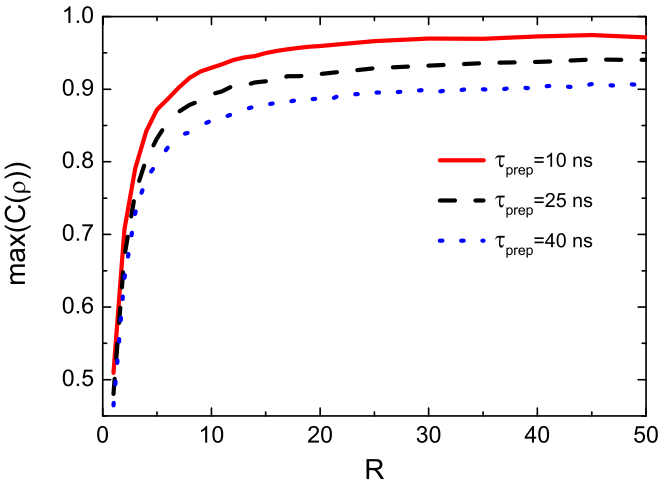

FIG. 5. Numerical solution for the maximum value of the concurrence as a function of R and for $\tau_{\text{prep}} = 10$ ns, $\tau_{\text{prep}} = 25$ ns, and $\tau_{\text{prep}} = 40$ ns, considering the description of the noise that better fits the experimental data, i.e., $\tau_c = 9$ ns and $J_0 = 11.6$ MHz.

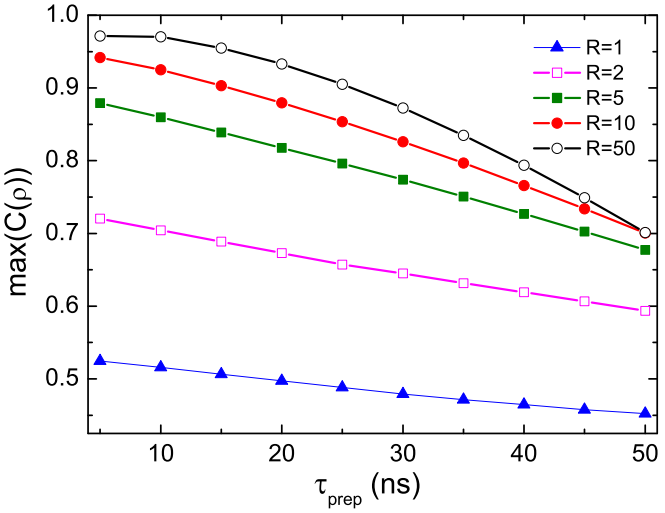

FIG. 6. Numerical solution for the maximum value of the concurrence as a function of τ_{prep} for $R = 1$, $R = 2$, $R = 5$, $R = 10$, and $R = 50$, considering the description of the noise that better fits the experimental data, i.e., $\tau_c = 9$ ns and $J_0 = 11.6$ MHz.

characteristic times that are intrinsically related to the success of achieving a maximally entangled state.

To illustrate the role of the preparation time and the dependency on the two-qubit coupling J_{12} in the entanglement dynamics, we plot in Fig. 5 the maximum value of concurrence as a function of $R = J_{12}/J_{12}^{\text{exp}}$, where J_{12}^{exp} is the value extracted from the experimental data, for different preparation times τ_{prep}. As expected, such results show an enhancement of the entanglement when J_{12} is increased and when τ_{prep} is decreased. This behavior is related to the fact that a maximally entangled configuration is faster achieved for a larger J_{12} even though the RTN disturbs the ideal obtainment of the superposed state during the preparation time τ_{prep}. In Fig. 5, one can see that for $R \gtrsim 20$ the maximum value of entanglement is approximately constant. Furthermore, a small increase in the value of J_{12} surprisingly enhances the maximum value of entanglement, as can be observed by the steep jump in $\max[C(\rho)]$ for a small variation of R in Fig. 5. To understand further how these characteristic times affect the maximally entangled state, in Fig. 6, we plot the maximum value of concurrence as a function of τ_{prep} for $R = 1$, $R = 2$, $R = 5$, $R = 10$, and $R = 50$. One can notice in Fig. 6 that the maximum concurrence monotonically decreases as a function of τ_{prep} and that the maximum concurrence rapidly increases with the increasing of R. For example, by doubling the experimental value of the two-qubit coupling ($R = 2$), the maximum value of entanglement has a growth of 40% for $5 \leqslant \tau_{\text{prep}} \leqslant 50$. These results address the way such physical parameters can be tuned in order to substantially enhance the entanglement between S-T_0 qubits.

IV. CONCLUSION

In summary, we proposed a model based on the RTN, which mimics the $1/f^{\alpha}$ noise, to describe the dissipative dynamics of two S-T_0 qubits in two DQDs. By employing such a model, we were able to determine a suitable description of the experimental data shown in Ref. [12]. Moreover, we studied the role of the preparation time and the two-qubit coupling in the dissipative dynamics. We showed that the two-qubit coupling plays a crucial role in the entanglement evolution and a small increase in J_{12} can lead to a considerable amplification of the entanglement. Such results can be used as a reference for further studies in quantum systems where the $1/f^{\alpha}$ noise is present.

ACKNOWLEDGMENTS

We thank M. Shulman and F. Brito for helpful discussions. L.K.C. and F.F.F. are grateful to the Brazilian Agencies FAPESP (Grants No. 12/13052-6 and No. 15/05581-7), CNPq (Grants No. 304841/2015-3 and No. 474592/2013-8), and CAPES for financial support. K.B. and F.F.F. would like to thank the International Centre for Theoretical Physics (ICTP) for financial support.

[1] M. Arcari, I. Sollner, A. Javadi, S. Lindskov Hansen, S. Mahmoodian, J. Liu, H. Thyrrestrup, E. H. Lee, J. D. Song, S. Stobbe, and P. Lodahl, Phys. Rev. Lett. **113**, 093603 (2014); R. Okamoto, J. L. O'Brien, H. F. Hofmann, T. Nagata, K. Sasaki, and S. Takeuchi, Science **323**, 483 (2009); S. Nadj-Perge, I. K. Drozdov, J. Li, H. Chen, S. Jeon, J. Seo, A. H. MacDonald, B. A. Bernevig, and A. Yazdani, *ibid.* **346**, 602 (2014); A. Fedorov, L. Steffen, M. Baur, M. P. da Silva, and A. Wallraff, Nature (London) **481**, 170 (2012); D. D. Awschalom, L. C. Bassett, A. S. Dzurak, E. L. Hu, and J. R. Petta, Science **339**, 1174 (2013); E. Togan, Y. Chu, A. S. Trifonov, L. Jiang, J. Maze, L. Childress, M. V. G. Dutt, A. S. Sorensen, P. R. Hemmer,

A. S. Zibrov, and M. D. Lukin, Nature (London) **466**, 730 (2010); W. B. Gao, P. Fallahi, E. Togan, J. Miguel-Sanchez, and A. Imamoglu, *ibid.* **491**, 426 (2012).
[2] D. Loss and D. P. DiVincenzo, Phys. Rev. A **57**, 120 (1998).
[3] A. Imamoglu, D. D. Awschalom, G. Burkard, D. P. DiVincenzo, D. Loss, M. Sherwin, and A. Small, Phys. Rev. Lett. **83**, 4204 (1999).
[4] D. Kim, S. G. Carter, Alex Greilich, Allan S. Bracker, and D. Gammon, Nat. Phys. **7**, 223 (2011).
[5] J. H. Jefferson, M. Fearn, D. L. J. Tipton, and T. P. Spiller, Phys. Rev. A **66**, 042328 (2002).
[6] C. Kloeffel and D. Loss, Annu. Rev. Condens. Matter Phys. **4**, 51 (2013).
[7] J. M. Taylor, J. R. Petta, A. C. Johnson, A. Yacoby, C. M. Marcus, and M. D. Lukin, Phys. Rev. B **76**, 035315 (2007).
[8] J. R. Petta, A. C. Johnson, J. M. Taylor, E. A. Laird, A. Yacoby, M. D. Lukin, C. M. Marcus, M. P. Hanson, and A. C. Gossard, Science **309**, 2180 (2005).
[9] J. Levy, Phys. Rev. Lett. **89**, 147902 (2002).
[10] B. M. Maune, M. G. Borselli, B. Huang, T. D. Ladd, P. W. Deelman, K. S. Holabird, A. A. Kiselev, I. Alvarado-Rodriguez, R. S. Ross, A. E. Schmitz, M. Sokolich, C. A. Watson, M. F. Gyure, and A. T. Hunter, Nature (London) **481**, 344 (2012).
[11] I. van Weperen, B. D. Armstrong, E. A. Laird, J. Medford, C. M. Marcus, M. P. Hanson, and A. C. Gossard, Phys. Rev. Lett. **107**, 030506 (2011).
[12] M. D. Shulman, O. E. Dial, S. P. Harvey, H. Bluhm, V. Umansky, and A. Yacoby, Science **336**, 202 (2012).
[13] O. E. Dial, M. D. Shulman, S. P. Harvey, H. Bluhm, V. Umansky, and A. Yacoby, Phys. Rev. Lett. **110**, 146804 (2013).
[14] V. Kornich, Christoph Kloeffel, and Daniel Loss, Phys. Rev. B **89**, 085410 (2014).
[15] P. Dutta and P. M. Horn, Rev. Mod. Phys. **53**, 497 (1981).
[16] A. V. Kuhlmann, J. Houel, A. Ludwig, L. Greuter, Dirk Reuter, A. D. Wieck, M. Poggio, and R. J. Warburton, Nat. Phys. **9**, 570 (2013).
[17] K. D. Petersson, J. R. Petta, H. Lu, and A. C. Gossard, Phys. Rev. Lett. **105**, 246804 (2010).
[18] M. Möttönen, Rogerio de Sousa, Jun Zhang, and K. B. Whaley, Phys. Rev. A **73**, 022332 (2006).
[19] G. Burkard, Phys. Rev. B **79**, 125317 (2009).
[20] D. Zhou, A. Lang, and R. Joynt, Quant. Inf. Proc. **9**, 727 (2010).
[21] P. Kuopanportti, M. Möttönen, V. Bergholm, O.-P. Saira, J. Zhang, and K. B. Whaley, Phys. Rev. A **77**, 032334 (2008).
[22] C. H. Bennett, G. Brassard, C. Crepeau, R. Jozsa, A. Peres, and W. K. Wootters, Phys. Rev. Lett. **70**, 1895 (1993).
[23] A. K. Ekert, Phys. Rev. Lett. **67**, 661 (1991).
[24] W. K. Wootters, Phys. Rev. Lett. **80**, 2245 (1998).
[25] In our numerical simulations, we used 3000 trajectories and a time step of $\Delta t = 1$ ns for all results, except for the results of Fig. 2, where we used 5000 trajectories and a time step of $\Delta t = 0.1$ ns.